Final Draft
of the original manuscript:

Campo, K.N.; Campanelli, L.C.; Bergmann, L.; dos Santos, J.F.; Bolfarini, C.:
Microstructure and interface characterization of dissimilar friction stir welded lap joints between Ti–6Al–4V and AISI 304
In: Materials and Design (2013) Elsevier

DOI: 10.1016/j.matdes.2013.11.002

Microstructure and interface characterization of dissimilar friction stir welded Ti-6Al-4V and AISI 304 austenitic stainless steel

Authors:
Kaio Niitsu Campo – Campo, K.N.[a]
Leonardo Contri Campanelli – Campanelli, L.C.[a]
Luciano Bergmann – Bergmann, L.[b]
Jorge Fernandez dos Santos – dos Santos, J.F.[b]
Claudemiro Bolfarini – Bolfarini, C.[a]

Affiliation:
[a]Federal University of São Carlos, Department of Materials Engineering, Rod. Washington Luiz km. 235, P.O. Box 676, 13565-905 São Carlos-SP, Brazil.
[b]Helmholtz-Zentrum Geesthacht, Institute of Materials Research, Materials Mechanics, Solid State Joining Processes (WMP), Max-Planck-Str. 1, D-21502 Geesthacht, Germany.

Abstract:
The feasibility of dissimilar friction stir welding between Ti-6Al-4V alloy and AISI 304 austenitic stainless steels was investigated. Sound joints were achieved when placing titanium as the upper workpiece of the lap configuration. Joints were successfully produced by employing a welding speed of 1 mm/s and rotational speeds of 300 and 500 rpm. A lamellar microstructure was formed in the stir zone of Ti-6Al-4V, where grain size was found to increase with increasing rotational speed, and austenitic equiaxed grains were obtained near the interface of 304 stainless steels coupon. SEM-EDS analysis of the interface revealed a thin intermixed region and suggested intermetallic compound formation. Microhardness data in the titanium weld zone for both rotational speeds exhibited slightly lower values than the base material, with the lowest values in the heat affected zone, whereas the microhardness values in the stainless steel side around the weld center were found to be higher than those obtained for the base material.

Keywords: Friction stir welding, dissimilar, titanium, stainless steel, microstructure, microhardness.

1. Introduction

Dissimilar joining between titanium alloys and stainless steels has attracted great interest in the aerospace, nuclear and chemical industries due to the high mechanical properties and corrosion resistance of them. Formation of brittle intermetallic compounds resulting from the limited solubility of Fe in α-Ti is the major drawback for joining these metals, with a greater complexity for austenitic stainless steels due to the possible development of complex phases involving Ti, Fe, Cr and Ni [1]. Conventional fusion welding is therefore limited by chemical and metallurgical incompatibilities [2], and so solid state welding processes have emerged as alternative since melting is avoided and formation of intermetallic compounds is reduced. Diffusion bonding has been employed for joining commercially pure titanium (CP-Ti) with AISI 304 stainless steel (304SS) by Ghosh et al. [3] and Ti-6Al-4V (Ti64) with micro-duplex stainless steel by Kundu et al. [4]. Despite the attempt to minimize intermetallic phases and therefore increase plasticity, maximum bond strength value achieved in both cases was 20-30% inferior to the strength of the respective weaker base material. Kurt et al. [5] characterized the interface of diffusion bonded Ti64 and 316SS. FeTi and Fe_2Ti were identified in the bonding region at any processing temperature and diffusion mechanism was more effective in the Ti coupon.

Friction stir welding (FSW) is a solid state welding technology with potential for joining dissimilar high-strength metals, as published for instance on A6061 Al alloy with 304SS [6], 5186 Al alloy with mild steel [7], 2024/7075 Al alloys with CP-Ti/Ti64 [8], and ZK60 Mg alloy with CP-Ti [9]. With respect to Ti and stainless steel, Fazel-Najafadabi et al. [10] attempted to place softer Ti over 304SS sheet, and the joint exhibited no adequate shear strength and plasticizing of the lap lower workpiece was not achieved. Tool rotation was increased to minimize the problem, but it resulted in oxygen pickup by the lap upper workpiece. In a second investigation [11], with 3044SS over Ti sheet, maximum shear strength was close to that of the lap weaker base material. Two joint mechanisms were suggested: chemical bonding at the interface with formation of a TiFe-based intermetallic compound and mechanical interlock regions at the joint interface of extruded stainless steel into the plasticized Ti. Dissimilar FSW of Ti64 and 304SS has not been reported in

the literature, and therefore the purpose of this work is to assess the possibility of achieving defect-free joints between these metals. The effect of process parameters on the integrity of the dissimilar weld has been investigated and microstructural zones and joint interface are characterized.

2. Experimental procedure

Sheets of Ti-6Al-4V (Ti64) and AISI 304 austenitic stainless steel (304SS) with 1.6 and 2.5 mm of thickness respectively were friction stir welded in lap joint configuration at room temperature without auxiliary preheating. An argon gas shielding was applied to protect against oxidation of the surface. A tungsten-lanthanum (W-La) tool consisting of a 25 mm diameter cylindrical shoulder and 13 mm diameter cylindrical pin was employed with a tilt angle of 2°. Tables 1 and 2 show the experimental chemical compositions of the as-received materials. Transverse weld cross-sections were cut by electrical discharge machining for metallographic analysis.

Table 1. Chemical composition of Ti64 sheets (wt.%).

Element	Ti	Al	V	Fe	O	C	H	Others
wt.%	Bal.	6.21	3.90	0.14	0.20	0.01	0.0045	< 0.40

Table 2. Chemical composition of 304SS sheets (wt.%).

Element	Fe	Cr	Ni	Mn	Si	C	N	P
wt.%	Bal.	18.40	8.15	1.60	0.42	0.08	0.05	0.03

After metallographic preparation, the 304SS coupon was electrolytically etched in a solution of 10% oxalic acid and 90% distilled water with a power supply set of 19 V during 18 s. Kroll reagent was used for etching the Ti64 coupon. Microstructure was characterized by optical microscopy (OM), as illustrated in Fig. 1 for the cross-sections of the as-received materials. Element distribution at the joint interface was investigated through energy dispersive X-ray spectroscopy (SEM-EDS). Vickers microhardness measurements were performed along the cross-sections using a conventional Vickers indenter with 0.5 kgf of load (or 25 gf close to the joint interface) during an indent period of 20 seconds. Microhardness profiles were determined at specific distances (1.0, 2.0 and 3.0 mm) from the bottom surface of each workpiece.

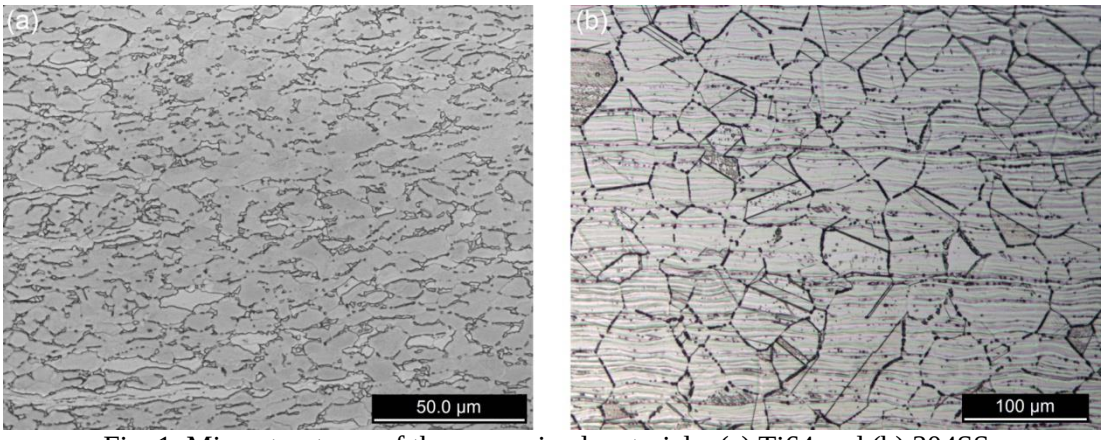

Fig. 1. Microstructures of the as-received materials: (a) Ti64 and (b) 304SS.

The initial levels of parameters were based on preliminary investigations and comprised 500 rpm of tool rotational speed, 2 mm/s of welding speed and 2.4 mm of plunge depth. Tool rotational and welding speeds were respectively varied between 300-500 rpm and 1-2 mm/s, whereas plunge depth was varied from 2.4 to 3.2 mm. 304SS sheet was initially tested as the lap upper workpiece and the results were unsatisfactory in the whole range of parameters. Fig. 2 illustrates the imperfect weld track with a notable surface discontinuity and a slight colorful appearance due to oxygen pickup. Further details regarding these observations are presented throughout the discussion. Ti64 sheets were therefore employed as the upper workpiece in the present study, and the specific combinations of parameters presented in Table 3 were investigated.

Fig. 2. Inadequate weld appearance obtained when placing 304SS as upper workpiece.

Table 3. Parameters specifications for Ti64 as upper workpiece.

Joint specification	Rotational speed (rpm)	Welding speed (mm/s)	Plunge depth (mm)
TiSS-1	500	2	2.4
TiSS-2	300	1	2.4
TiSS-3	500	1	2.4

3. Results and discussion

Low magnification overviews of the welded joints are presented in Fig. 3. The weld seam exhibits a satisfactory visual aspect in all samples, although a colorful pattern indicative of partial oxidation was observed in TiSS-1 and TiSS-3. Cross-section macrograph of TiSS-1 (Fig. 3(a)) shows a pronounced lack of consolidation at the advancing side as a consequence of insufficient heat input. According to the torque-based approach reported by Lombard et al. [12] and considering a process efficiency of 60% [13], heat input values were calculated and presented in Table 4. The energy introduced for plasticization and flow of Ti was 41 and 66% larger for TiSS-2 and TiSS-3 respectively in comparison to TiSS-1, in which the higher welding speed reduces the dwell time at high-temperature. A curved boundary resulting from the flow of material is created at the interface in the actuation radius of tool pin, which is better visualized on the macrograph at the advancing side as a sharp protuberance. The thickness of the sheets in the center of the joint presents a variation among the samples, which might be correlated with heat input levels. The higher value in TiSS-3 is an indicative of improved heat transfer to 304SS sheet and therefore the Ti64 sheet is slightly ticker in this case (1.60 mm against 1.48 mm in TiSS-2).

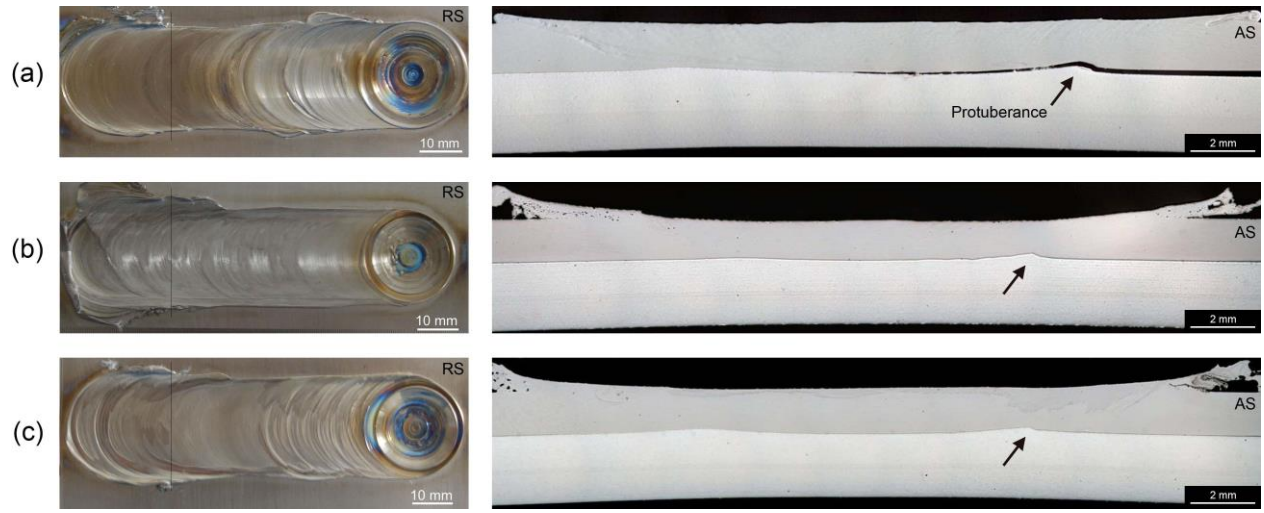

Fig. 3. Macrographs of top surface and cross-section of samples: (a) TiSS-1, (b) TiSS-2 and (c) TiSS-3.

Table 4. Calculated heat input values.

Joint specification	Heat input (J/mm)
TiSS-1	1013
TiSS-2	1426

Process output responses, introduced in Fig. 4 as torque and axial load, are complementary tools to determine the most effective FSW parameters. The stability of the welding process for sound joints is in principle reflected by the continuity of the torque profile. The pronounced oscillation observed for the TiSS-1 weld indicates that the process is not stable along the joint, which means that the welding system had difficulties on maintaining the tool rotational speed due to the lack of adequate plasticization of the material. It is inferred from the load chart that a high axial force is required for the development of the welding process, varying from 25 kN (51 MPa, considering the shoulder diameter as an approximation of the axial loaded section) for TiSS-1 to a maximum of 40 kN (81 MPa) for TiSS-2. Although temperature measurements were not performed in this work, values around the 1100°C achieved in the interface by Fazel-Najafabadi [10] are expected, in which the Ti64 yield strength can reach 330 MPa [14] and can be lower than 50 MPa for 304SS [15]. The superior magnitude of process related stresses in comparison to the steel yield strength at the operating temperature leads to an excessive plasticization and dragging of material when 304SS is placed as upper workpiece (Fig. 2).

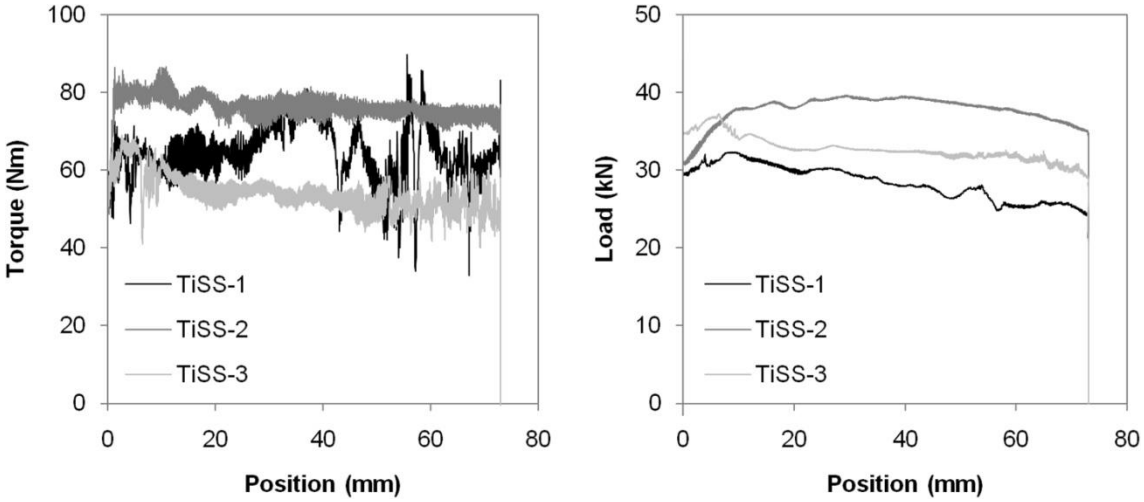

Fig. 4. Process diagrams of torque and axial load versus position of the welded joint.

A typical etched cross-section macrograph is presented in Fig. 5 (TiSS-2), where three main regions are distinguishable through optical contrast: stir zone (SZ), heat affected zone (HAZ) and base material (BM). Fig. 6 illustrates the microstructures of the welding zones. SZ is similar to the microstructures observed by Zhou et al. [16] for high rotational speeds, which consist of prior β grains in the form of lamellar α/β colonies and grain boundary α as a consequence of phase transformation with cooling from single β-field. Average grain size increases from 9,1 μm for TiSS-2 to 12,3 μm for TiSS-3 against 8,7 μm of BM, suggesting that SZ of Ti64 coupon is only subjected to dynamic recovery during the welding procedure. Grain coarsening in TiSS-3 results from the greater heat input (higher peak temperature and longer dwell time above β-transus) produced by the higher rotational speed. As observed in Fig. 6(c), the transition between HAZ and SZ is very sharp, indicating that the thermo-mechanically affected zone (TMAZ) is not observed in Ti64 workpiece [17]. Similar to BM (Fig. 1(a)), the HAZ microstructure is characterized by equiaxed primary α in a matrix of transformed β, with a higher volume fraction of β phase than in BM, and is almost not changed with tool rotational speed, which means that temperature in this zone is below β-transus and dwell time is not appreciable [16]. An investigation of the light phase outlined in Fig. 5 through SEM-EDS revealed the presence of W resulting from the wear of the FSW tool during the welding.

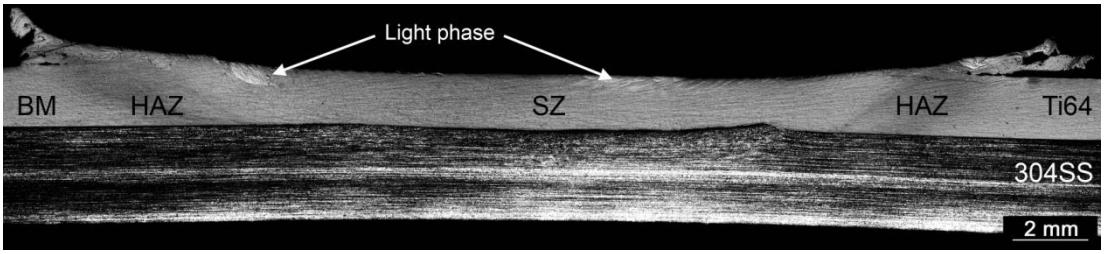

Fig. 5. Cross-section macrograph of a typical Ti64/304SS joint with the various regions.

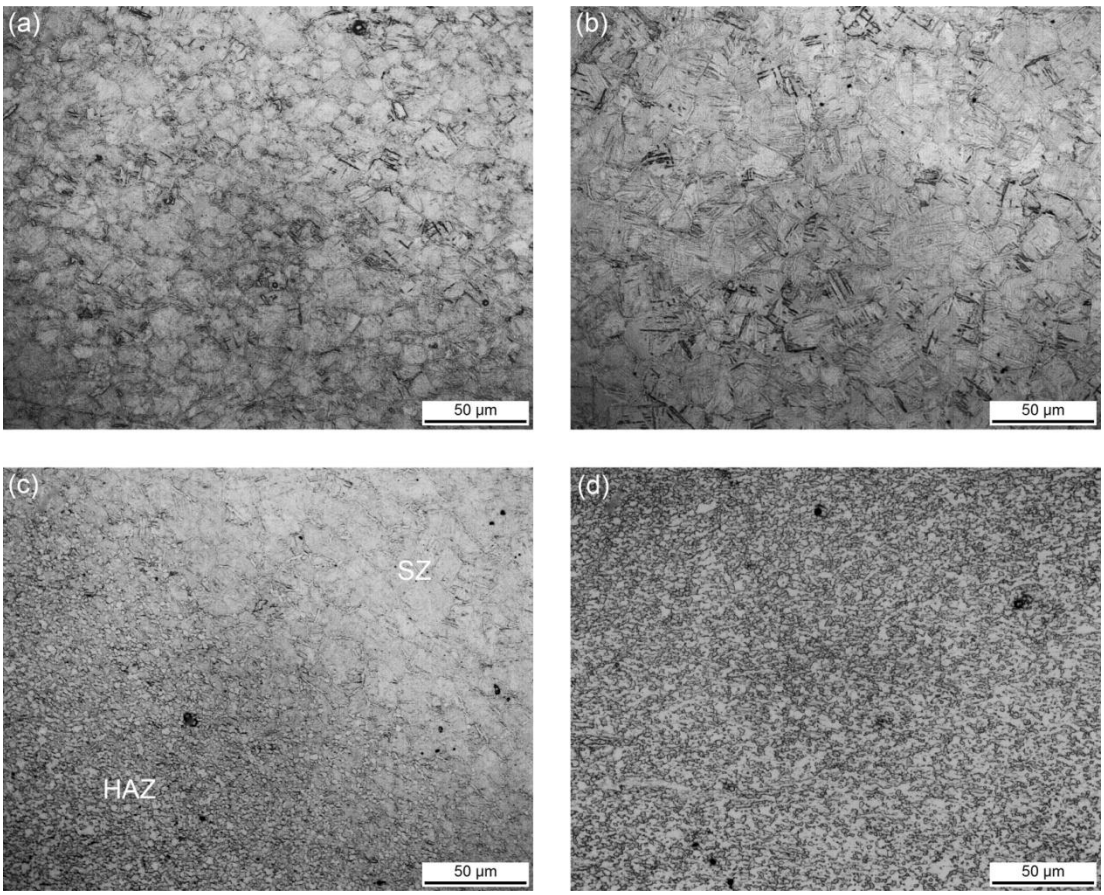

Fig. 6. Microstructures of Ti64 sheet: (a) SZ of TiSS-2, (b) SZ of TiSS-3, (c) transition between HAZ and SZ and (d) typical HAZ.

Although the tool did not plunge into the 304SS sheet, microstructure in the center of the joint varies in comparison to BM, as shown in Fig. 7 for TiSS-2. Refined austenite grains are observed near the interface, with an average grain size of 11,0 µm against 26,7 µm of BM, and therefore it is believed that dynamic recrystallization occurs as a consequence of the high deformation rate and the thermal cycle imposed by the process, combined with the low stacking fault energy of γ-Fe close-packed structure. Other evidence is the reduced amount of twinning in the SZ against a heavy twin structure in the non-affected BM. As reported by Fazel-Najafadabi et al. [11], grain boundaries are serrated since this region is subjected to a severe degree of plastic deformation. With increasing distance from the interface to the opposite free surface of the sheet, microstructure becomes more equiaxed (although still heterogeneous) and average grain size increases up to around the BM grain size, suggesting that BM structure (Fig. 1(b)) is maintained in the bottom portion of the sheet due to the negligible effects of the process.

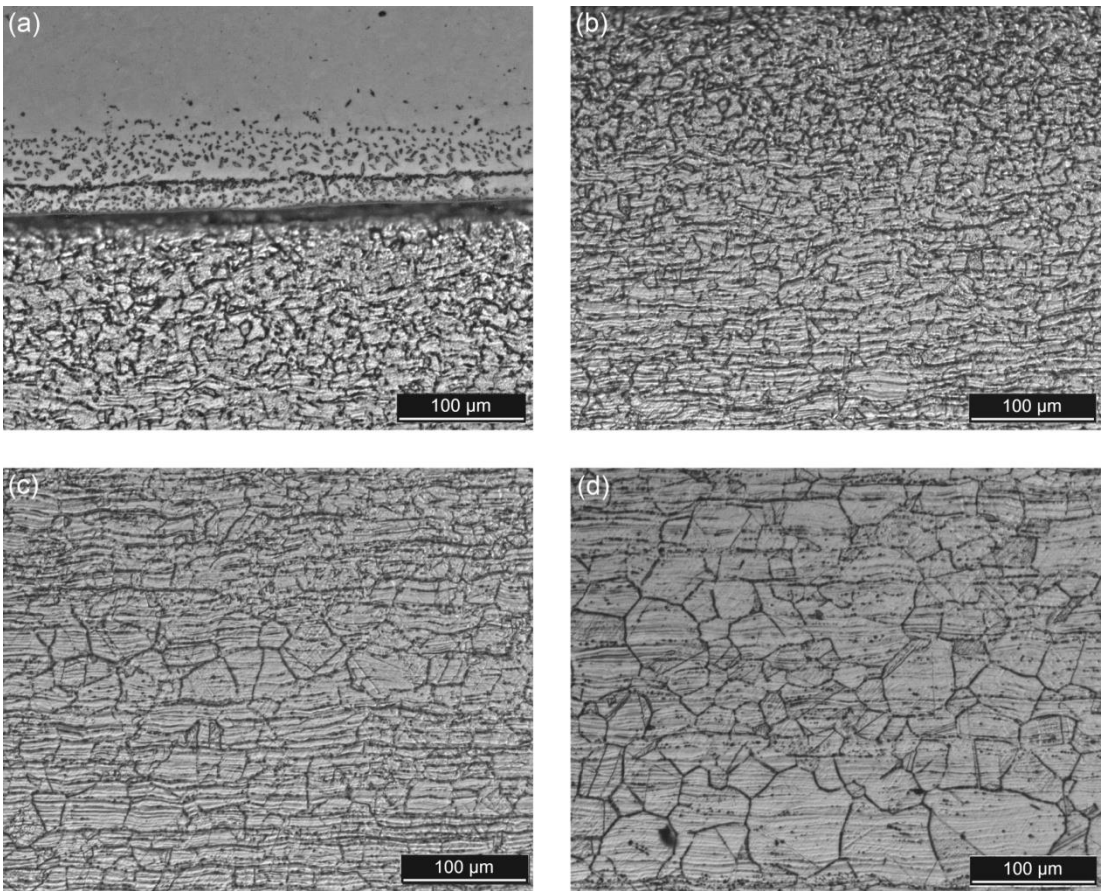

Fig. 7. Microstructures of 304SS sheet: (a) near the interface; (b), (c) and (d) increasing distance from the interface.

Vickers microhardness profile across the 304SS sheet of TiSS-2 is shown in Fig. 8. The microstructure refinement in the vicinity of the weld center is responsible for the increased hardness in comparison to BM. The highest values are observed in the region under direct effect of the tool pin, where the magnitude of plastic deformation is intensified, and therefore a continuous reduction is noticed with increasing the distance from the weld center. Hardness values are slightly higher in the 2.0 mm line, which is consistent with the improved grain refinement near the interface that results from dynamic recrystallization. A similar microhardness profile has also been observed for the specimen TiSS-3 welded with higher rotational speed, since no significant changes in the microstructure have been observed.

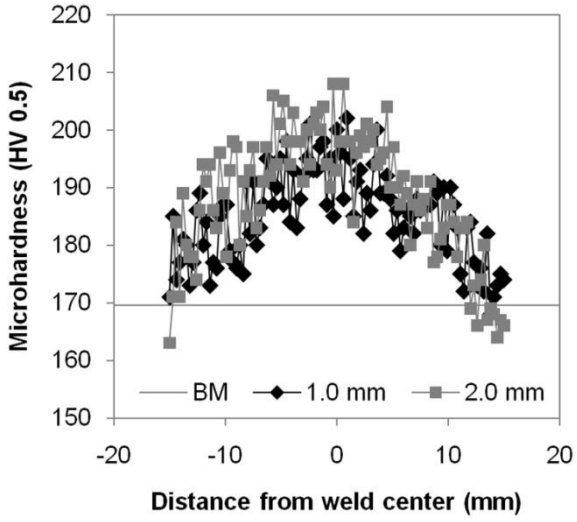

Fig. 8. Microhardness profile along 304SS sheet.

Fig. 9 presents the microhardness distributions across the Ti64 sheet at 3.0 mm distant from the bottom surface and Table 4 brings mean and standard deviation values for the different zones. Despite the small

variation in microhardness along SZ, mean values are slightly lower than BM possibly due to a dynamic recovery process and consequent reduction in dislocation density. The differences among both samples are not statistically significant, although lower mean hardness could be expected for TiSS-3 due to grain coarsening. Particularly in TiSS-3, peaks associated to contamination with tool material are observed in the advancing side (reaching values up to 383 HV), suggesting that tool wear was more pronounced in higher rotational speeds. Softening is noticed in the HAZ as a consequence of a higher volume fraction of β phase, corresponding to a reduction of 7 and 5% in comparison to BM respectively for TiSS-2 and TiSS-3. The higher heat input in TiSS-3 results in a slightly higher fraction of transformed β than TiSS-2, however sufficient to an additional decrease in the mean hardness. Microstructural equivalence between advancing and retreating sides explains the similar profile in both regions.

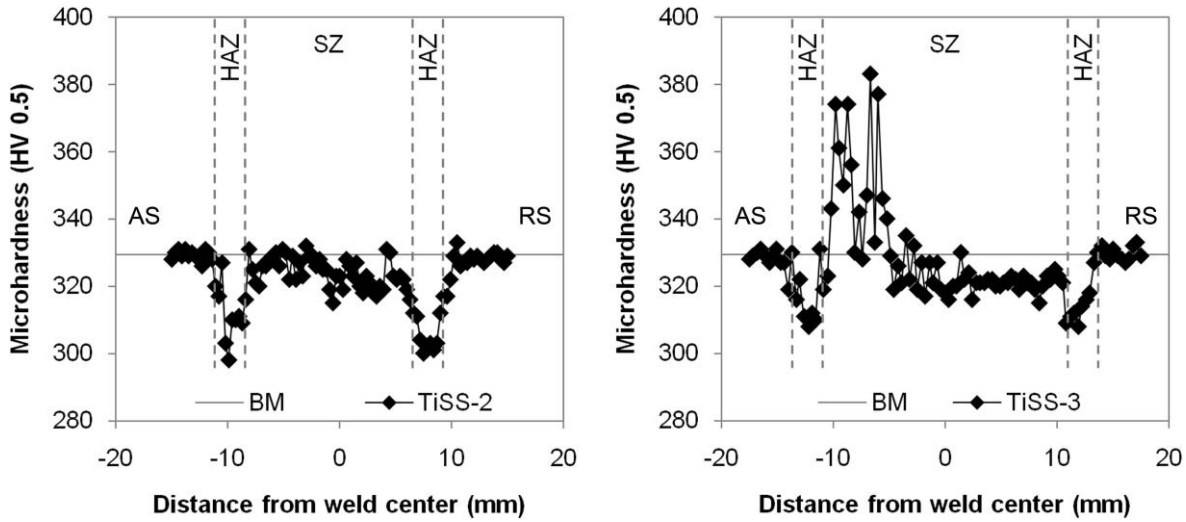

Fig 9. Microhardness profile along Ti64 sheet at 3.0 mm from the bottom surface of the joints.

Table 4. Microhardness average and standard deviation at Ti64 sheet.

Sample	HV 0.5			
	BM	HAZ AS	HAZ RS	SZ
TiSS-2	329 ± 4	307 ± 5	305 ± 5	324 ± 5
TiSS-3		313 ± 5	313 ± 4	322 ± 4*

*Not considering the peak values.

Fig. 10 illustrates a SEM-EDS line scan across the interface of TiSS-2 and the average concentration profile of the main chemical species. Detailed mapping distribution is presented in Fig. 11. The expected processing temperature (above 1100°C, as previously mentioned) causes the diffusion of the elements through the interface, generating a thin intermixed region (IMR) of approximately 5 μm width, which is constant throughout the interface and mostly placed in the Ti64 side, and an intermetallic phase zone in the 304SS side. While 304SS preserves the face-centered cubic structure above 1100°C, Ti64 turns from hexagonal close packed to body-centered cubic (β-transus around 990°C) [3]. The more open structure of Ti64 at high temperature allows a more effective diffusion of Fe, Cr and Ni into Ti64 sheet than the penetration of the other elements into the steel sheet. Average chemical composition close to the interface in Ti64 correspond to 58%Ti-22%Fe-6%Cr-4%Al-3%Ni-3%V (wt.%), and a layer of β phase may be retained inside IMR at room temperature due to the diffusion of strong β-stabilizer elements from stainless steel. The microhardness of 228 ± 14 HV measured in this specific region against 329 ± 4 of BM (see Table 4) is indicative of β phase occurrence, as expected for a region of single body-centered cubic phase. Regarding the 304SS side, 55%Fe-17%Cr-14%Ti-5%Ni-1%Al-1%V (wt.%) is the average composition right next IMR, which suggests the formation of intermetallic Fe_2Ti according to Fe-Cr-Ti phase diagram (peak in Ti line distribution). Similar analysis of TiSS-3 also provided an IMR of about 5 μm width, indicating that, although a higher heat input may improve the motility of the alloying elements, the dwell time was not sufficient to cause any significant increase in the diffusion distance.

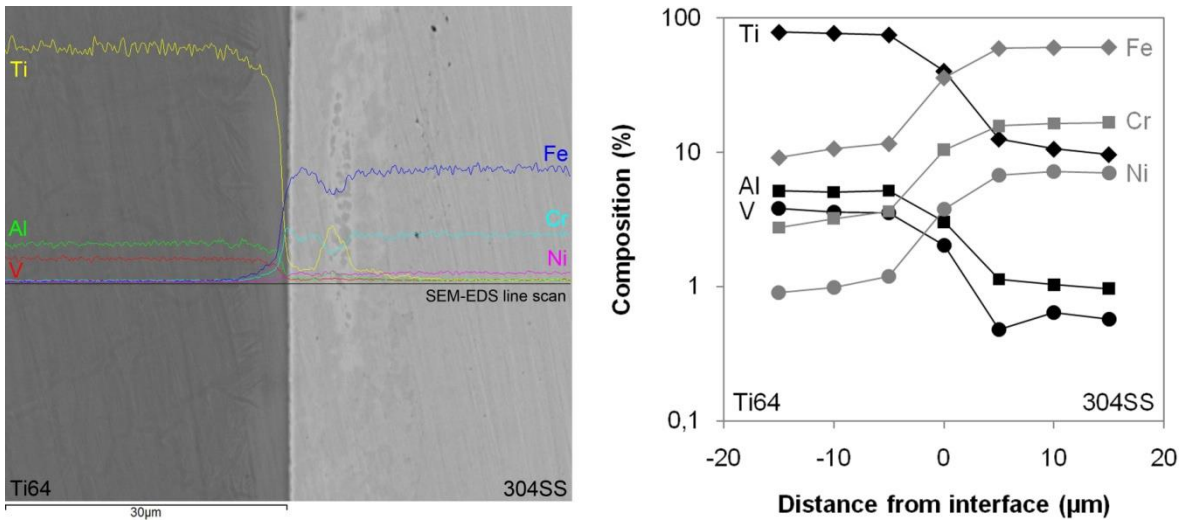

Fig. 10. SEM-EDS line scan distribution and concentration profiles of the main elements across the interface

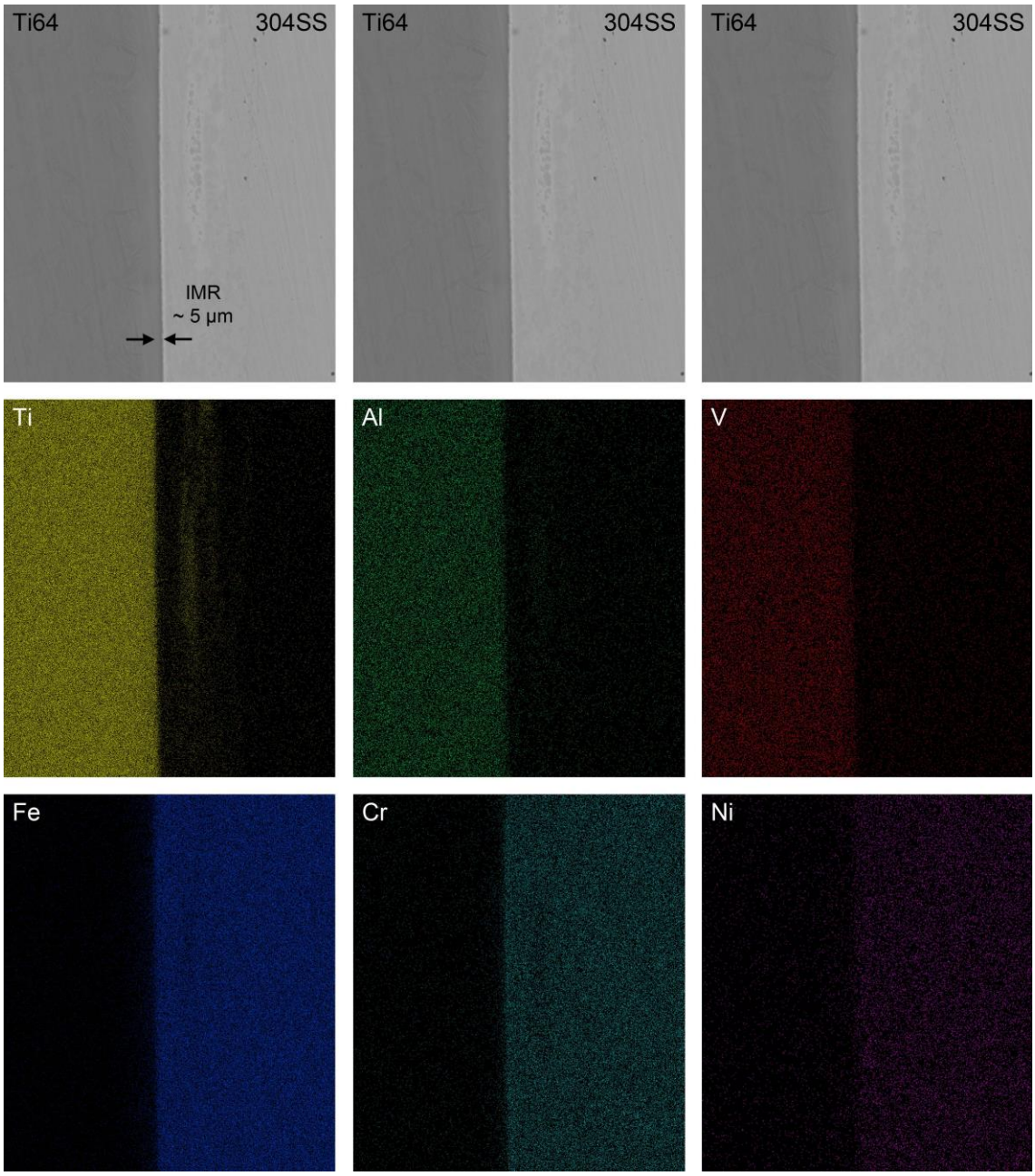

Fig. 11. SEM-EDS mapping distribution of the main elements across the interface.

Conclusions

1. Defect-free dissimilar joints were successfully achieved at a constant welding speed of 1 mm/s with rotational speeds above 300 rpm by placing Ti64 as upper workpiece due to the higher strength of the former at the processing temperature. A minimum level of heat input resulting from the combination of welding parameters was necessary to guarantee a defect-free weld.

2. Ti64 sheet was directly affected by the tool motion and two welding zones were generated besides the unaffected BM. SZ was characterized by dynamically recovered lamellar α/β colonies, and a small grain coarsening was observed with increasing tool rotational speed, although the effect on reducing microhardness was not considerable. The microstructure in the HAZ consisting of equiaxed primary α in a matrix of transformed β promoted a significant drop in microhardness distribution due to a higher volume fraction of β phase when compared to BM and was not changed in the employed range of parameters.

3. With regard to the 304SS sheet, refined austenite grains almost free of twinning was indicative of dynamic recrystallization in the vicinity of the joint interface, which resulted in a microhardness profile of the welding zone superior to BM. Appreciable grain coarsening was identified with moving away from the interface as a consequence of the reduced driving force for recrystallization.

4. Interface characterization suggested the stabilization of β phase at room temperature and formation of intermetallic Fe_2Ti respectively at Ti64 and 304SS sides. Intermixed region width was almost not changed with rotational speed since dwell time is short to improve the diffusion distance even with the higher level of heat input.

Acknowledgements

The authors would like to thank Mr. T. Leonhard for supplying the material for the tool. We are also indebted to CCDM (Materials Development and Characterization Center) – Brazil, for the assistance with scanning electron microscopy.

References

[1] Tomashchuk I, Sallamand P, Andrzejewski H, Grevey D. The formation of intermetallics in dissimilar Ti6Al4V/copper/AISI 316 L electron beam and Nd:YAG laser joints. Intermetallics 2011;19:1466-73.
[2] Fuji A, Ameyama K, North TH. Improved mechanical properties in dissimilar Ti-AISI 304L joints. J Mater Sci 1996;31:819-27.
[3] Ghosh M, Chatterjee S. Effect of interface microstructure on the bond strength of the diffusion welded joints between titanium and stainless steel. Mater Charact 2005;54:327-37.
[4] Kundu S, Sam S, Chatterjee S. Evaluation of interface microstructure and mechanical properties of the diffusion bonded joints of Ti-6Al-4V alloy to micro-duplex stainless steel. Mater Sci Eng A 2011;528:4910-16.
[5] Kurt B, Orhan N, Kaya M. Interface characterisation of diffusion bonded Ti-6Al-4V alloy and austenitic stainless steel couple. Mater Sci Tech 2009;25(4):556-60.
[6] Ogura T, Nishida T, Tanaka Y, Nishida H, Yoshikawa S, Fujimoto M, et al. Microscale evaluation of mechanical properties of friction stir welded A6061 aluminium alloy/304 stainless steel dissimilar lap joint. Sci Technol Weld Joi 2013;18(2):108-13.
[7] Dehghani M, Amadeh A, Akbari Mousavi SAA. Investigations on the effects of friction stir welding parameters on intermetallic and defect formation in joining aluminum alloy to mild steel. Mater Design 2013;49:433-41.
[8] Aonuma M, Nakata K. Dissimilar metal joining of 2024 and 7075 aluminium alloys to titanium alloys by friction stir welding. Mater Trans 2011;52(5):948-52.
[9] Aonuma M, Nakata K. Dissimilar metal joining of ZK60 magnesium alloy and titanium by friction stir welding. Mater Sci Eng B 2012;177:543-48.
[10] Fazel-Najafabadi M, Kashani-Bozorg SF, Zarei-Hanzaki A. Joining of CP-Ti to 304 stainless steel using friction stir welding technique. Mater Design 2010;31:4800-07.
[11] Fazel-Najafabadi M, Kashani-Bozorg SF, Zarei-Hanzaki A. Dissimilar lap joining of 304 stainless steel to CP-Ti employing friction stir welding. Mater Design 2011;32;1824-32.
[12] Lombard H, Hattingh DG, Steuwer A, James MN. Optimising FSW process parameters to minimise defects and maximise fatigue life in 5083-H321 aluminium alloy. Eng Fract Mech 2008;75:341-54.
[13] Lienert TJ, Stellwag Jr WL, Lehman LR. Comparison of heat inputs: friction stir welding vs. arc welding. [Internet] Available from: http://174.122.108.74/conferences/abstracts/2002/011.pdf

[14] Lee W-S, Lin C-F. High-temperature deformation behaviour of Ti6Al4V alloy evaluated by high strain-rate compression tests. J Mater Process Tech 1998;75:127-36.
[15] Mäkeläinen P, Outinen J. Mechanical properties of an austenitic stainless steel at elevated temperatures. J Constr Steel Res 1998;46(1-3):455. Paper no. 101.
[16] Zhou L, Liu HJ, Liu QW. Effect of rotation speed on microstructure and mechanical properties of Ti-6Al-4V friction stir welded joints. Mater Design 2010;31:2631-36.
[17] Zhang Y, Sato YS, Kokawa H, Park SHC, Hirano S. Microstructural characteristics and mechanical properties of Ti-6Al-4V friction stir welds. Mater Sci Eng A 2008;485:448-55.